Acta Crystallographica Section F
Structural Biology and Crystallization Communications
ISSN 1744-3091

Conformational bias imposed by source microseeds results in structural ambiguity

Netanel Tzarum,[b] David Engelberg[a] and Oded Livnah[b]*

[a]The Department of Biological Chemistry, The Alexander Silberman Institute of Life Sciences, The Hebrew University of Jerusalem, Jerusalem 91904, Israel, and [b]The Wolfson Centre for Applied Structural Biology, The Hebrew University of Jerusalem, Jerusalem 91904, Israel

Correspondence e-mail: oded.livnah@huji.ac.il

Received 29 March 2011
Accepted 12 May 2011

The p38 MAP kinase pathway is an essential component of numerous cellular signalling networks which are usually activated in response to extracellular environmental stress conditions. In addition to the canonical activation, several alternative activation pathways have been identified for p38; one of these, in which p38 is initially phosphorylated on Tyr323 and consequently autoactivated, is exclusive to T cells and is induced by TCR activation. Intrinsically active and inactive mutants at position 323 have been developed in order to evaluate the structural changes that occur upon TCR-induced activation. In order to promote crystal growth, cross streak-seeding techniques were utilized. This technique has gained popularity in promoting crystal growth when spontaneous nucleation induces critical defects or is being entirely hindered. The crystal characteristics of some mutants were highly similar to those of the wild-type source seeds (form *A*). In contrast, other mutants crystallized spontaneously with a different space group and molecular packing (form *B*). One of the active mutants (Y323T) crystallized in both crystal forms, displaying different packing characteristics and significant differences in molecular conformation that were clearly dictated by the source seeds. This implies that the source seeds used in cross streak-seeding could, in some cases, impose bias on the structural outcome of the studied molecule. Such incidents could occur when the conformational freedom permits crystal packing while not reflecting the authentic structure.

1. Introduction

p38 mitogen-activated protein (MAP) kinases function in numerous signalling processes and are pivotal to the normal functioning of cells and organisms (Eckert *et al.*, 2003; Hu *et al.*, 1999; Shi & Gaestel, 2002). Abnormal p38 activity is associated with inflammatory diseases (Han *et al.*, 1994; Lee *et al.*, 1994; Sabapathy *et al.*, 2001) and cancers (Engelberg, 2004; Haq & Zanke, 1998; Harkin *et al.*, 1999; Lee *et al.*, 2000; Recio & Merlino, 2002). The p38 subfamily consists of four isoforms, α, β, γ and δ, which share high sequence similarity (Jiang *et al.*, 1997). As a result of extracellular stimuli, p38s are commonly activated by a unique activation mechanism that requires dual phosphorylation of a Tyr-Gly-Tyr motif located on the activation loop by the upstream activator MAP kinase kinase (MKK). This activation results in an increase in activity by three orders of magnitude (Widmann *et al.*, 1999; Fig. 1). In addition to the canonical activation pathway, three MKK-independent alternative activation pathways have been described in recent years (Ge *et al.*, 2002; Gills *et al.*, 2007; Salvador *et al.*, 2005). One of them, which is exclusive to T cells and is mediated by T-cell receptor (TCR) activation, involves the phosphorylation of p38α and p38β at a novel phosphorylation site Tyr323 located in the L16 loop region (Fig. 1*b*), distal to the activation loop, by ZAP-70 tyrosine kinase. Subsequent to phosphorylation, p38α attains autophosphorylation capabilities and becomes activated (Mittelstadt *et al.*, 2009; Fig. 1*a*). The structural alterations on p38 activation in the canonical and alternative pathways are mainly unclear owing to a lack of relevant models. However, it has recently been shown that utilizing intrinsically active variants of p38α and subsequent structural studies could be a valuable tool in understanding their mechanism of activation (Diskin *et al.*, 2004; Diskin,

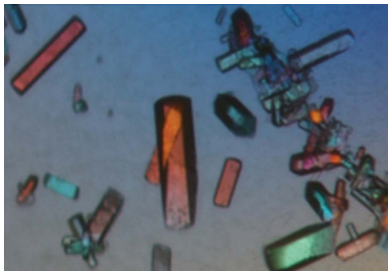

Lebendiker *et al.*, 2007). Using an analogous approach, we elected to mutate Tyr323 to the remaining 19 amino acids and assayed the activities of the mutants. Several of the mutants at position 323 ($p38\alpha^{Y323A}$, $p38\alpha^{Y323D}$, $p38\alpha^{Y323Q}$, $p38\alpha^{Y323R}$ and $p38\alpha^{Y323T}$) displayed intrinsic activity capable of phosphorylating a p38-specific substrate, ATF2 (Tzarum *et al.*, 2011). Two mutants, $p38\alpha^{Y323F}$ and $p38\alpha^{Y323W}$, displayed a lower activity compared with the low activity of the non-activated wild-type p38α. In order to reveal the activation mechanism, the three most active mutants ($p38\alpha^{Y323Q}$, $p38\alpha^{Y323T}$ and $p38\alpha^{Y323R}$) and one inactive mutant ($p38\alpha^{Y323F}$) were selected for structural studies and their structures were determined (Tzarum *et al.*, 2011).

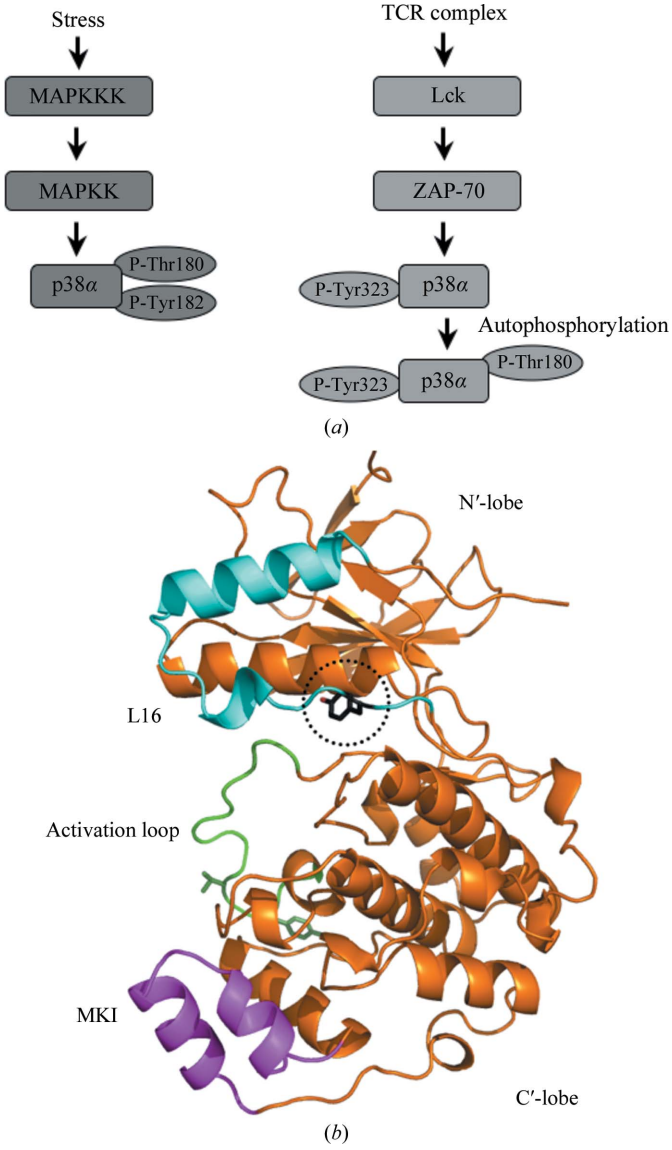

Figure 1
(*a*) Schematic diagram of p38α activation pathways. The three-tiered MAP kinase canonical pathway results in dual phosporylation on neighbouring Thr180 and Tyr182 phosphoacceptors (p38α numbering) located on the phosphorylation lip (left). The MAP kinases are activated by MAPKK, which in turn is activated by MAPKKK. The alternative TCR activation-induced p38 pathway (right), exclusive to T cells, results in phosphorylation of p38α/β by ZAP-70 tyrosine kinase on a novel phosphorylation site, Tyr323. Subsequent to Tyr323 phosphorylation, p38α is autoactivated and monophosphorylated on Thr180. (*b*) A ribbon cartoon of p38α (PDB entry 1p38; Wang *et al.*, 1997) showing the overall topology of the N′- and C′-lobes, which form a catalytic groove between them. The phosphorylation lip containing the TGY motif located between the lobes and the L16 loop region which is part of the C-terminal extension are shown in green and cyan, respectively. The alternative phosphorylation site (Tyr323) located in L16 is coloured black and is highlighted by a dotted circle. The MAP kinase insert, which is a signature feature of the MAP kinase family and is located at the edge of the C′-lobe, is shown in magenta. All molecular-graphics figures were generated using *PyMOL* (DeLano, 2002).

Obtaining well diffracting crystals is imperative for structure determination *via* X-ray crystallographic methods. The initial step in crystal growth is the formation of stable and ordered crystalline nuclei, which are the starting point for the growth of mature crystals (Salemme *et al.*, 1988; Jullien *et al.*, 1994). In numerous instances such nuclei do not form spontaneously despite the high degree of supersaturation and metastable conditions and thus require the incorporation of crystal seeds that serve as initiators for the growth of macrocrystals. These methods involve the introduction of either macroseeds or microseeds into a pre-equilibrated crystallization experiment (Thaller *et al.*, 1981; Fitzgerald & Madsen, 1986). One of the most convenient and effective microseeding techniques is streak-seeding (Stura & Wilson, 1990; Bergfors, 2003). In this method, microcrystal seeds are removed from the source crystals using a whisker or fibre and then streak-seeded into the target crystallization experiment. When the seeds grow into mature crystals, the path of the streak can usually be clearly followed. This method can be also extended to cross-seeding, in which microseeds or nuclei of one protein are transferred into a target solution containing a mutated or highly similar protein and/or a protein–ligand complex (Stura *et al.*, 1992). In some cases, owing to differences in chemical properties, alterations of crystallization conditions are also required in order to permit the propagation of crystal growth (Stura *et al.*, 1992).

In this work, we describe the crystallization procedures for four p38α position-323 mutants (active and inactive) by utilizing cross streak-seeding methods. Initially, when cross-seeding an active mutant in which the mutated amino acid was relatively smaller than the original residue, such as $p38\alpha^{Y323T}$, the resulting crystals were biased by the source seeds, as they maintained the same crystallographic parameters and crystal-packing contacts. In contrast, a similar cross-seeding procedure with active mutants with large and polar residues ($p38\alpha^{Y323Q}$ and $p38\alpha^{Y323R}$) using wild-type crystals as the source did not succeed. Spontaneous crystals of $p38^{Y323R}$ were obtained but with a different morphology and crystal packing that accommodates the mutated molecules (form *B*). Consequent cross-seeding was applied to the position-323 active mutants using the new crystals as the source seeds. The $p38\alpha^{Y323T}$ mutant also crystallizes with the form *B* morphology. The two crystal forms resulted in different models of the active $p38\alpha^{Y323T}$ displaying significant conformational changes representing the bias induced by the source seeds.

2. Materials and methods

The expression, purification and crystallization of all of the human p38α variants (UniProtKB code Q16539; MW = 41.3 kDa) was performed as described previously (Tzarum *et al.*, 2011; Diskin, Engelberg *et al.*, 2007; Diskin, Lebendiker *et al.*, 2007). We elected to crystallize the position-323 mutants using crystallization conditions similar to those used for the previously crystallized wild-type p38α ($p38\alpha^{wt}$) and p38α active mutants ($p38\alpha^{D176A}$, $p38\alpha^{D176A+F327L}$ and $p38\alpha^{D176A+F327S}$) using streak-seeding in order to enhance crystal growth (Diskin, Engelberg *et al.*, 2007; Diskin, Lebendiker *et al.*, 2007). Crystals of all mutants were obtained using the sitting-drop vapour-diffusion technique in 24-well Linbro plates (Hampton Research) at 277 K with 1 ml reservoir solution and a 6 µl crystal-

Table 1
Data-collection and refinement statistics.

Values in parentheses are for the last shell.

	p38α^{Y323F}	p38α^{Y323T} (form *A*)	p38α^{Y323T} (form *B*)	p38α^{Y323R}	p38α^{Y323Q}	p38α^{wt}†	p38$\alpha^{D176A+F327S}$†
ESRF beamline	ID23-1	ID23-1	ID29	ID29	ID29	ID29	ID29
Wavelength (Å)	0.9300	0.9300	0.9300	0.9300	0.9300	0.9800	1.0600
Space group	$P2_12_12_1$	$P2_12_12_1$	$P2_1$	$P2_1$	$P2_1$	$P2_12_12_1$	$P2_12_12_1$
Unit-cell parameters (Å, °)	a = 64.7, b = 69.0, c = 74.4	a = 67.2, b = 74.8, c = 78.9	a = 40.3, b = 71.7, c = 70.9, β = 90.3	a = 40.0, b = 72.3, c = 68.9, β = 105.0	a = 37.9, b = 71.8, c = 63.5, β = 95.2	a = 69.1, b = 69.8, c = 74.3	a = 67.2, b = 69.4, c = 74.4
Resolution range (Å)	50–1.6 (1.66–1.60)	50–2.1 (2.18–2.10)	50–2.7 (2.75–2.70)	50–2.3 (2.34–2.30)	50–2.2 (2.24–2.20)	50–2.0 (1.83–1.80)	50–2.2 (2.24–2.20)
V_M (Å^3 Da^{-1})	2.10	2.45	2.57	2.40	2.15	2.24	2.07
Solvent content (%)	41.6	50	52	49	42	45	40
Unique reflections	44536	23757	11304	16552	16913	34244	18295
Multiplicity	7.7	5.5	3.1	3.6	3.3	4.6	5.0
R_{merge} (%)	4.3 (75.8)	6.1 (60.7)	8.4 (56.6)	9.4 (80.6)	7.2 (59.7)	5.1 (47.2)	6.6 (65.7)
Completeness (%)	99.9 (99.4)	99.2 (96.8)	99.0 (99.5)	97.5 (96.9)	98.2 (95.7)	99.7 (99.8)	99.2 (99.6)
$\langle I/\sigma(I)\rangle$	29.0 (1.3)	30.5 (1.6)	16.3 (1.8)	21.2 (2.3)	22.4 (2.6)	35.0 (3.2)	30.4 (1.2)
No. of protein atoms	2711	2684	2781	2709	2604		
No. of β-OG atoms	40	40	20	40	20		
No. of solvent atoms	333	216	22	23	12		
R factor	0.183	0.220	0.200	0.214	0.222		
R_{free} (5% of data)	0.223	0.281	0.283	0.281	0.304		
Average B factor (Å^2)							
Protein	25.8	45.3	60.3	60.9	55.8		
β-OG	28.1	67.6	57.8	66.0	66.8		
Solvent	38.7	49.4	40.8	52.8	41.9		
R.m.s.d. from ideality							
Bond lengths (Å)	0.011	0.011	0.015	0.013	0.012		
Bond angles (°)	1.39	1.31	1.66	1.66	1.43		
Ramachandran plot (*PROCHECK*)							
Favoured (%)	90.7	96.6	85.6	86.4	84.0		
Allowed (%)	9.0	3.4	14.1	13.3	15.3		
Generously allowed (%)	0.3	0.0	0.3	0.3	0.7		
Disallowed (%)	0.0	0.0	0.0	0.0	0.0		

† These structures were not fully refined.

lization drop consisting of equal amounts of protein and reservoir solution. Streak-seeding was performed with a cat whisker, which was used to touch the source crystals and was then dragged through previously equilibrated drops. In addition, when crystals of the active mutants were not obtained, we conducted a screen of several dozen new conditions with and without microseeding, which resulted in no crystal growth. Prior to data collection, the crystals of p38α^{Y323F}, form *A* of p38α^{Y323T}, p38α^{wt} and p38$\alpha^{D176A+F327S}$ were cryoprotected using Paratone-N oil (Hampton Research) and immediately flash-cooled in liquid nitrogen. The crystals of p38α^{Y323Q}, p38α^{Y323R} and form *B* of p38α^{Y323T} were cryoprotected using the reservoir solution with the addition of 20% glycerol.

Crystallographic data for p38α^{wt} and all mutants were collected on the ID23-1 and ID29 beamlines at the European Synchrotron Radiation Facility (ESRF) using an ADSC Quantum 315r CCD detector. The data for all crystals were integrated and scaled using the *HKL* suite (Otwinowski & Minor, 1997). The crystals of p38α^{wt}, p38$\alpha^{D176A+F327S}$, p38α^{Y323F} and form *A* of p38α^{Y323T} belonged to the orthorhombic space group $P2_12_12_1$ with one molecule per asymmetric unit. The crystals of p38α^{Y323Q}, p38α^{Y323R} and form *B* of p38α^{Y323T} belonged to the monoclinic space group $P2_1$ with one p38α molecule in the asymmetric unit (Table 1). The unit-cell parameters of the active mutants were not identical, but they all have a structure with highly similar crystal packing that can be categorized into the form *B* group. For each mutant several crystals were examined that displayed similar crystallographic properties and the highest quality data are reported. The structures of p38α^{Y323F} and form *A* of p38α^{Y323T} were solved *via* molecular-replacement methods using *MOLREP* (Vagin & Teplyakov, 2010) as implemented in *CCP*4 (Winn *et al.*, 2011) using the previously reported structure of p38α (PDB entry 2fso; Diskin, Lebendiker *et al.*, 2007) as the search model after removing all solvent and detergent molecules. The structure was refined using *REFMAC*5 (Murshudov *et al.*, 2011) and solvent molecules were added utilizing *ARP*/*wARP* (Morris *et al.*, 2003). The structure was fitted to electron-density maps using the graphics program *Coot* (Emsley & Cowtan, 2004). The structure of p38α^{Y323R} was solved *via* molecular-replacement methods using *MOLREP* with the structure of p38α^{Y323F} as the search model. The solved structure was then refined by *REFMAC*5 (Murshudov *et al.*, 2011). The subsequent stages were performed as described above. The structures of p38α^{Y323Q} and of form *B* of p38α^{Y323T} were solved *via* molecular-replacement methods using the refined model of p38α^{Y323R} as a search model (Tzarum *et al.*, 2011). The atomic coordinates and structure factors have been deposited in the PDB with accession codes 3od6, 3ody, 3odz and 3oef for the Y323T, Y323Q, Y323R and Y323F mutants, respectively.

3. Results and conclusions

Based on previous crystallization results, we attempted to crystallize four different position-323 p38α mutants applying conditions similar to those successfully used to obtain p38α^{wt} crystals (Diskin, Engelberg *et al.*, 2007; Diskin, Lebendiker *et al.*, 2007). The cross streak-seeding method was used in order to induce crystallization using the p38α^{wt} crystals as a source of microseeds (Stura *et al.*, 1992). The first protein to crystallize was the inactive p38α^{Y323F} mutant, using the previously described reservoir solution consisting of 17%(*w*/*v*) PEG 3350, 0.1 *M* HEPES pH 7.25, 0.2 *M* potassium fluoride and 25 m*M* *n*-octyl-β-D-glucopyranoside (β-OG). After 4 h of equilibration at 277 K, streak-seeding using p38α^{wt} crystals was conducted in order to initiate crystallization. Crystals of p38α^{Y323F} appeared within 2–3 d of seeding. They displayed similar morphology to those of p38α^{wt} (Fig. 2*a*); however, they diffracted poorly. An additive screen was employed and the diffraction improved after the addition of 20 m*M*

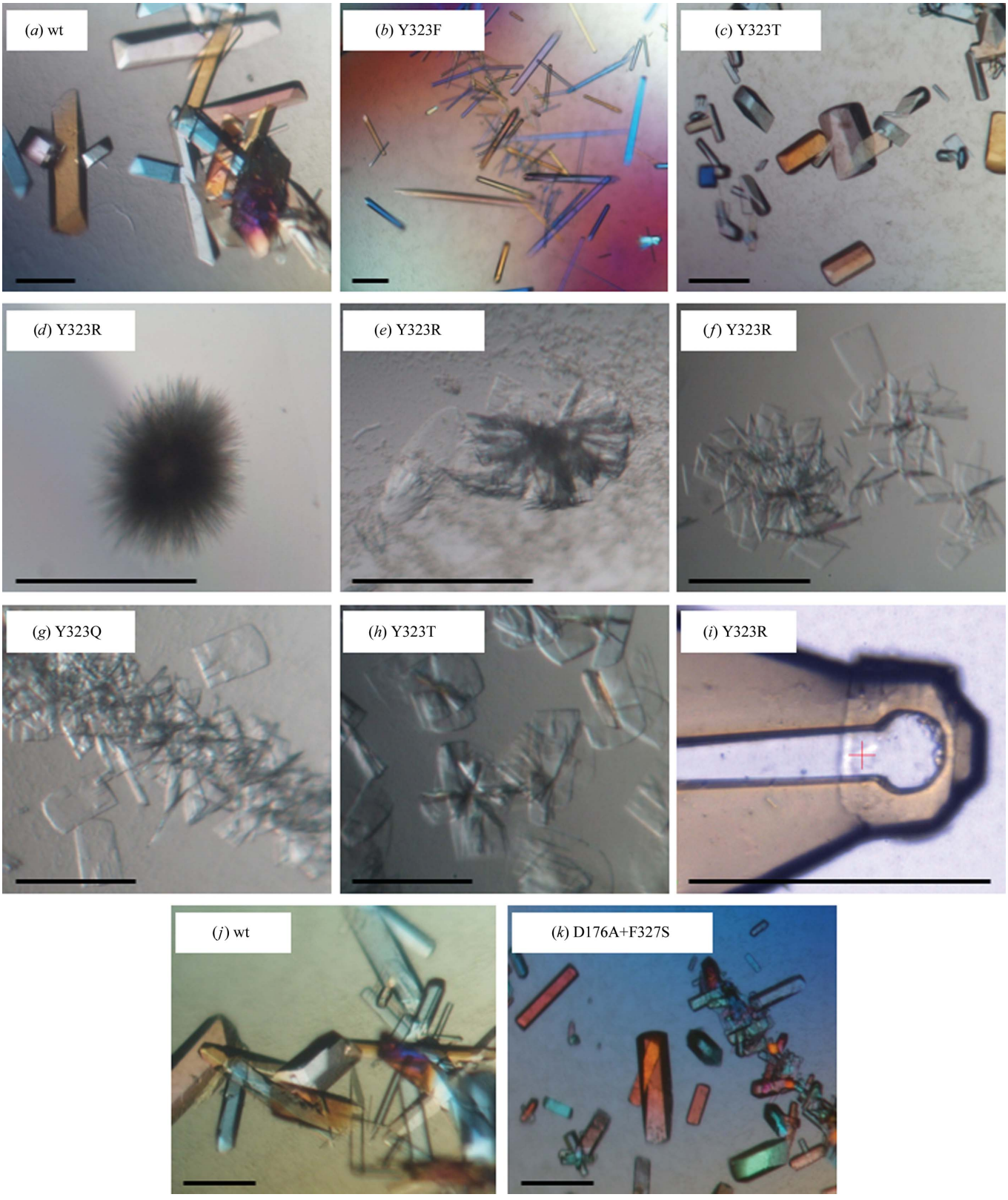

Figure 2
(*a*) Crystals of p38α^{wt}, which also provided the source seeds for streak-seeding of p38α^{Y323F} (*b*) and p38α^{Y323T} (*c*). The mutant crystals display high similarity to the p38α^{wt} morphology, belonging to the orthorhombic $P2_12_12_1$ space group (form *A*). (*d*) Cluster of needle-like crystals of the p38α^{Y323R} active mutant which appeared spontaneously. Optimization of the crystallization conditions resulted in thin plate-like crystals (*e*). (*f*) Using these crystals as a source for streak-seeding resulted in plate-like crystal clusters which were then optimized to individual plates. (*g*, *h*) The crystallization of the p38α^{Y323Q} (*g*) and p38α^{Y323T} (*h*) active mutants was performed using similar crystallization conditions as for p38α^{Y323R} using crystals of the p38α^{Y323R} mutant as a source of seeds. For p38α^{Y323Q}, the trace of the streak can be followed (*g*). (*i*) The Tyr323 active mutants belonged to the monoclinic space group $P2_1$ (form *B*) and reached final dimensions of 60× 40 × 2 µm (*i*). (*j*, *k*) Crystals of p38α^{wt} (*j*) and the intrinsically active mutant p38$\alpha^{D176A+F323S}$ (*k*) streak-seeded from the form *B* p38^{Y323R} crystals belonged to space group $P2_12_12_1$ (form *A*). The bar in each figure corresponds to 0.1 mm.

$AlCl_3$ to the reservoir solution (Fig. 2*b*). Crystals of the p38α^{Y323T} mutant which exhibited similar morphology to those of p38α^{Y323F} and p38α^{wt} appeared after 3–4 d using a reservoir solution consisting of 17%(*w*/*v*) PEG 3350, 0.1 *M* HEPES pH 7.0, 0.2 *M* potassium fluoride and 25 m*M* β-OG (Fig. 2*c*).

The resultant crystal structures of the p38α^{Y323T} and p38α^{Y323F} mutants belonged to space group $P2_12_12_1$ and displayed highly similar crystal packing to that observed for p38α^{wt}, defined as form *A* (Table 1). Their overall models maintained the two-lobe MAPK topology with no substantial changes in the mutation site or interlobe orientation. These structures have considerable crystal contacts near position 323 and the L16 loop region (Diskin, Engelberg *et al.*, 2007; Diskin, Lebendiker *et al.*, 2007; Fig. 3*a*).

Crystallization of active mutants bearing larger amino acids at position 323, p38α^{Y323Q} and p38α^{Y323R}, displayed different crystallization behaviour to p38α^{wt}. More specifically, the initial crystallization trials were conducted similarly to those for p38α^{Y323F} and p38α^{Y323T} as described above. However, 1–2 d after streak-seeding extensive precipitation appeared without apparent crystals. After 8–10 d spherical clusters of needle-like crystals appeared sporadically (Fig. 2*d*). We assumed that these crystals grew spontaneously and not as a result of the seeding owing to the time of growth and morphology and as these crystals did not appear to grow along the seeding path (streak). Moreover, crystallization experiments on the mutants without seeding resulted in similar needle-like crystals, which appeared spontaneously after 7–10 d. These crystals were too small for diffraction studies and we therefore attempted to refine the conditions in order to enlarge them. Consequently, crystals appeared after optimizing the crystallization conditions (19% PEG 3350, 0.1 *M* HEPES pH 7.75, 0.1 *M* potassium fluoride and 25 m*M* β-OG) but were still too small. These crystals were then used for streak-seeding, resulting in plate-like crystal clusters (Fig. 2*e*) which were then optimized *via* additional seeding cycles, resulting in individual plate-like crystals (Fig. 2*f*). The p38α^{Y323Q} and p38α^{Y323R} mutants crystallized in a different space group (form *B*) to p38α^{Y323F} and p38α^{wt} and exhibited different crystal packing in comparison to that observed in form *A* (Figs. 2*g* and 3*b*; Table 1). In the p38α^{Y323Q} and p38α^{Y323R} mutants the mutated residues at position 323 are too large and polar to accommodate the pocket originally occupied by Tyr323. Accordingly, the corresponding residues are now directed outwards, thus interrupting the original form *A* crystal packing and consequently inducing different crystal contacts (defined as form *B*; Tzarum *et al.*, 2011). These results are in agreement with our initial concept of why the p38α^{Y323Q} and p38α^{Y323R} mutants did not crystallize in form *A*.

The dichotomy in the properties of p38α^{Y323T}, which is an activating mutant yet still maintains the overall structure of the inactive form *A*, brought us to the primary assumption that the solved crystal structure does not accurately present the true conformational state.

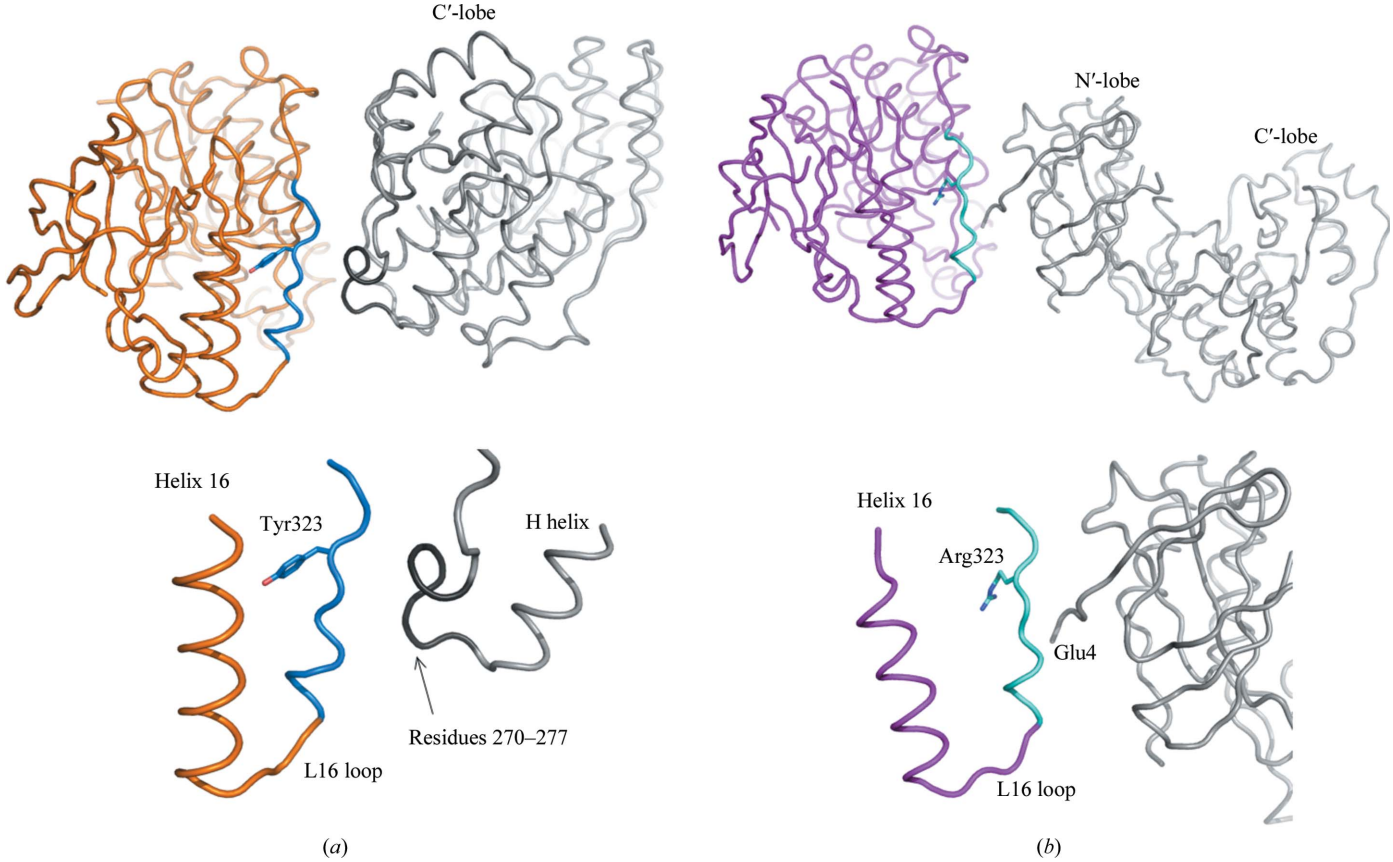

Figure 3
(*a*) Crystal contacts in the vicinity of the Tyr323 and L16 loop (highlighted in cyan) region of the N-lobe of p38α (orange). The displayed p38α^{wt} crystal contacts (top) with the symmetry-related partner [shown in grey and generated by the $-x + 0.5, -y, z + 0.5$ symmetry operator and a translation of (0, 1, 1)] in the vicinity of L16 are representative of p38α^{Y323F}, p38$\alpha^{D176A+F327S/L}$ and form *A* of p38α^{Y323T}. An enlargement of the contact region (bottom) shows part of the L16 region that forms interactions with the loop connecting the α2L14 helix and the H helix (residues 270–277) located in the C-lobe of the symmetry-related molecule. (*b*) For the position-323 active mutants represented by the Y323R mutant the crystal packing is drastically different compared with that displayed for the form *A* packing (top). The L16 loop region shown in cyan forms hardly any interactions with the symmetry-related molecule. The enlarged contact area (bottom) is displayed for clarity, emphasizing that only a short segment of the N-terminus of the symmetry-related molecule is located in the vicinity of L16 [shown in grey and generated by the $-x + 0.5, -y, z + 0.5$ symmetry operator and a translation of (1, −1, 1)]. The two packing configurations of the two p38 crystal forms exhibit entirely different characteristics, providing different conformational restrictions on the L16 loop.

We thus examined the possibility that the resultant crystals present in form *A* could be dictated by crystal packing of the source seeds. As discussed above, the form *A* crystal packing in p38α^{wt} and p38α^{Y323F} exhibits close crystal contacts between the L16 loop region near position 323 and the symmetry-related partner of a loop connecting α2L14 and the H-helix (residues 270–277) part of the MAP kinase insert (MKI) region (Fig. 3*a*). In the p38α^{Y323T} mutation threonine has a relatively small side chain which can easily accommodate the pocket previously occupied by tyrosine. In this context, it is possible that although the protein in solution has an active conformation it can undergo a conformational change upon crystallization in order to satisfy the packing restraints of the wild-type source seeds.

In order to test the assumption that p38α^{Y323T} could crystallize in both the inactive form *A* and the active form *B* depending upon which cross-seeding source was used, we attempted to crystallize the p38α^{Y323T} mutant using the same crystallization conditions as the p38α^{Y323Q} and p38α^{Y323R} active mutants. Streak-seeding was conducted using the plate-like crystals of p38α^{Y323R} as source crystals. These crystallizations resulted in p38α^{Y323T} crystals which appeared after 7 d and were clearly visible along the cross-seeding streak and that had a similar morphology to the other active mutants designated as form *B* (Fig. 2*h*). The X-ray structures of form *B* p38α^{Y323T} exhibit similar crystal packing, belonging to the monoclinic space group $P2_1$ and having highly similar structural characteristics to the p38α^{Y323R} and p38α^{Y323Q} active mutants (Tzarum *et al.*, 2011; Table 1). In this context, structural analysis revealed that the active mutants display dramatic conformational changes in the kinase interlobe orientation in comparison to p38α^{wt}, the inactive p38α^{Y323F} mutant and form *A* of p38α^{Y323T} (Fig. 4*a*; Tzarum *et al.*, 2011). In addition, there were also local changes in the L16 loop region near position 323 (Fig. 4*b*). These results appear to indicate that the crystal form adopted by p38α^{Y323T} (either the inactive form *A* or the active form *B*) is induced by the source microseeds.

In order to investigate whether p38α^{Y323T} crystallized in both forms owing to the size of the mutated residue and the possible plasticity of the resultant structure, we further examined cross-seeding using the reverse approach. In this case, we used source seeds of p38^{Y323R} mutant which grew in the form *B* morphology and cross-seeded them into solutions containing p38α^{wt} and the intrinsically active mutant p38$\alpha^{D176A+F323S}$. The crystal structure of this intrinsically active mutant, which has autophosphorylation capabilities, exhibits the characteristics of form *A* (Diskin *et al.*, 2004; Diskin, Lebendiker *et al.*, 2007). Crystals appeared along the streak after slightly fine-tuning the conditions with a similar morphology as

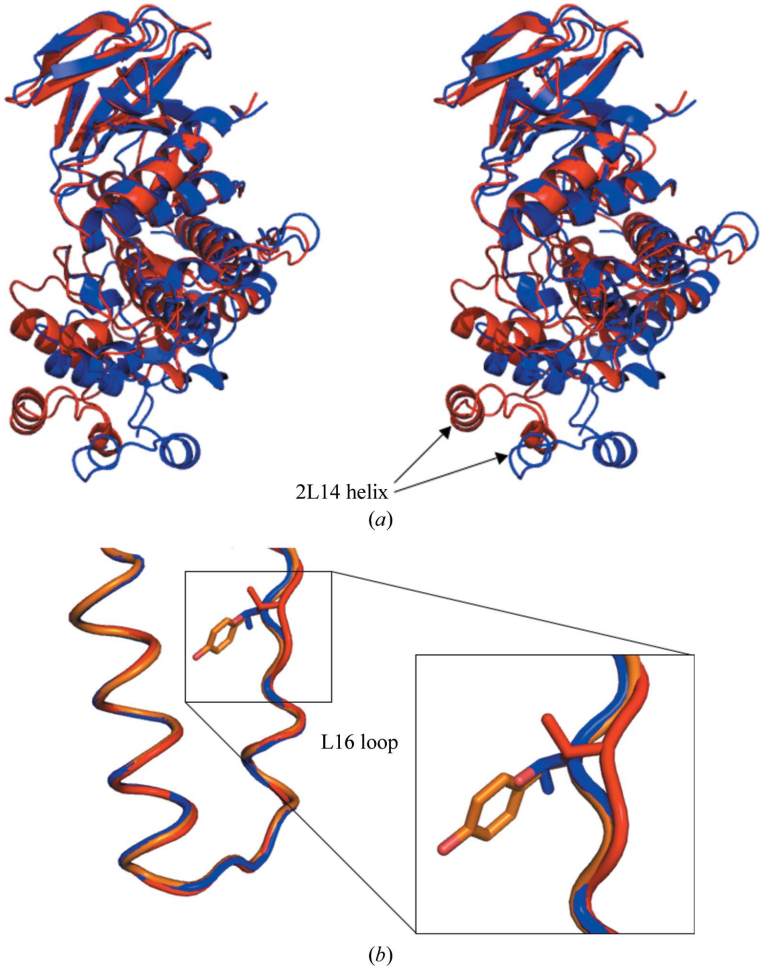

Figure 4
(*a*) Superposition of ribbon representations of the two p38α^{Y323T} forms (blue and red for forms *A* and *B*, respectively). The two models are superimposed on the N-lobes, emphasizing the differences in the C-lobe positions between the two models. The arrows indicate the positions of the α2L14 helix from the MAP kinase insert region, which shifts by 12 Å between the two crystals (measured from Gln253 C^{α}). (*b*) In form *A* Thr323 (blue) and the L16 loop follow the part of the position previously occupied by Tyr323 (orange). The main chain of the L16 loop region in the vicinity of Thr323 (form *B*, red) adopts a different conformation compared with the wild type and form *A* of p38α^{Y323T}, shifting the threonine residue to a different position.

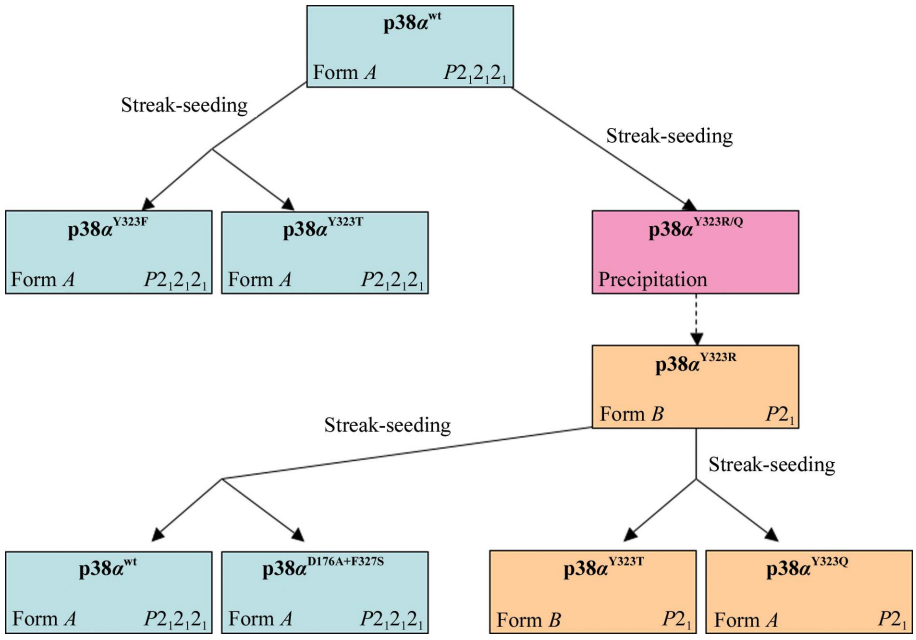

Figure 5
Flowchart of the course of crystallization of p38α active mutants. p38α^{wt} crystals belonging to space group $P2_12_12_1$ (form *A*) were used as a source seeds for streak-seeding into crystallization experiments of the Tyr323 mutants. The resultant crystals of the p38α^{Y323F} and p38α^{Y323T} mutants belonged to space group $P2_12_12_1$, with similar crystal packing as the wild type. Conversely, a similar approach for the p38α^{Y323Q} and p38α^{Y323R} mutants resulted in extensive precipitation, with the spontaneous formation of needle-like crystals after several weeks. Optimization of the crystallization conditions and streak-seeding from the latter crystals resulted in p38α^{Y323R} crystals belonging to the monoclinic space group $P2_1$ (form *B*). Crystals with similar morphology were also obtained *via* streak-seeding for the p38α^{Y323Q} and p38α^{Y323T} mutants and belonged to space group $P2_1$. Utilization of streak-seeding into assays containing p38α^{wt} and the p38$\alpha^{D176A+F327S}$ mutant using the form *B* p38α^{Y323R} crystals resulted in form *A* crystals belonging to space group $P2_12_12_1$.

previously obtained (Diskin, Engelberg *et al.*, 2007; Diskin, Lebendiker *et al.*, 2007; Figs. 2*j*, 2*k* and 5). Diffraction data and preliminary structural solution revealed that although the source microseeds belonged to the active form *B*, space group $P2_1$, in both cases the mature crystals had the form *A* $P2_12_12_1$ symmetry with the original wild-type and D176A+F323S structural features and crystal contacts (Diskin, Engelberg *et al.*, 2007; Diskin, Lebendiker *et al.*, 2007). In the p38α^{Y323T} mutant the small threonine side chain, although polar, can apparently be accommodated in the large pocket previously occupied by tyrosine and the restraints imposed by the source seeds result in a conformational shift satisfying the form *A* packing.

One can thus conclude that when the protein conformation cannot adjust to the crystal-packing restraints induced by the source seeds it will direct the crystallization outcome towards its inherent and cognate profile. For structures that can adapt to the conformation of the source seeds, the resultant crystal form may be dictated by their properties. For the p38α^{Y323T} mutant there was conformational freedom that could permit alterations to both forms, with the source seed thus imposing bias on the resulting crystal form and consequently the structural features. Thus, the conformation observed in the crystal structure resulting from cross streak-seeding may not always reflect its structural status in solution and should be further evaluated by examining crystal-packing considerations of the source crystals.

This research was supported by the Israel Science Foundation grant 630/07 and Israel Science Foundation Research Center of Excellence 180/09 awarded to OL and DE.

References

Bergfors, T. (2003). *J. Struct. Biol.* **142**, 66–76.
DeLano, W. L. (2002). *PyMOL*. http://www.pymol.org.
Diskin, R., Askari, N., Capone, R., Engelberg, D. & Livnah, O. (2004). *J. Biol. Chem.* **279**, 47040–47049.
Diskin, R., Engelberg, D. & Livnah, O. (2007). *Acta Cryst.* D**63**, 260–265.
Diskin, R., Lebendiker, M., Engelberg, D. & Livnah, O. (2007). *J. Mol. Biol.* **365**, 66–76.
Eckert, R. L., Efimova, T., Balasubramanian, S., Crish, J. F., Bone, F. & Dashti, S. (2003). *J. Invest. Dermatol.* **120**, 823–828.
Emsley, P. & Cowtan, K. (2004). *Acta Cryst.* D**60**, 2126–2132.
Engelberg, D. (2004). *Semin. Cancer Biol.* **14**, 271–282.
Fitzgerald, P. M. D. & Madsen, N. B. (1986). *J. Cryst. Growth*, **76**, 600–606.
Ge, B., Gram, H., Di Padova, F., Huang, B., New, L., Ulevitch, R. J., Luo, Y. & Han, J. (2002). *Science*, **295**, 1291–1294.
Gills, J. J., Castillo, S. S., Zhang, C., Petukhov, P. A., Memmott, R. M., Hollingshead, M., Warfel, N., Han, J., Kozikowski, A. P. & Dennis, P. A. (2007). *J. Biol. Chem.* **282**, 27020–27029.
Han, J., Lee, J. D., Bibbs, L. & Ulevitch, R. J. (1994). *Science*, **265**, 808–811.
Haq, R. & Zanke, B. (1998). *Cancer Metastasis Rev.* **17**, 233–239.
Harkin, D. P., Bean, J. M., Miklos, D., Song, Y.-H., Truong, V. B., Englert, C., Christians, F. C., Ellisen, L. W., Maheswaran, S., Oliner, J. D. & Haber, D. A. (1999). *Cell*, **97**, 575–586.
Hu, M. C., Wang, Y., Mikhail, A., Qiu, W. R. & Tan, T.-H. (1999). *J. Biol. Chem.* **274**, 7095–7102.
Jiang, Y., Gram, H., Zhao, M., New, L., Gu, J., Feng, L., Di Padova, F., Ulevitch, R. J. & Han, J. (1997). *J. Biol. Chem.* **272**, 30122–30128.
Jullien, M., Crosio, M.-P., Baudet-Nessler, S., Mérola, F. & Brochon, J.-C. (1994). *Acta Cryst.* D**50**, 398–403.
Lee, J. C., Kumar, S., Griswold, D. E., Underwood, D. C., Votta, B. J. & Adams, J. L. (2000). *Immunopharmacology*, **47**, 185–201.
Lee, J. C., Laydon, J. T., McDonnell, P. C., Gallagher, T. F., Kumar, S., Green, D., McNulty, D., Blumenthal, M. J., Heys, J. R. & Landvatter, S. W. (1994). *Nature (London)*, **372**, 739–746.
Mittelstadt, P. R., Yamaguchi, H., Appella, E. & Ashwell, J. D. (2009). *J. Biol. Chem.* **284**, 15469–15474.
Morris, R. J., Perrakis, A. & Lamzin, V. S. (2003). *Methods Enzymol.* **374**, 229–244.

Murshudov, G. N., Skubák, P., Lebedev, A. A., Pannu, N. S., Steiner, R. A., Nicholls, R. A., Winn, M. D., Long, F. & Vagin, A. A. (2011). *Acta Cryst.* D**67**, 355–367.
Otwinowski, Z. & Minor, W. (1997). *Methods Enzymol.* **276**, 307–326.
Recio, J. A. & Merlino, G. (2002). *Oncogene*, **21**, 1000–1008.
Sabapathy, K., Kallunki, T., David, J. P., Graef, I., Karin, M. & Wagner, E. F. (2001). *J. Exp. Med.* **193**, 317–328.
Salemme, F., Genieser, R. L., Finzel, B. C., Hilmer, R. M. & Wendoloski, J. J. (1988). *J. Cryst. Growth*, **90**, 273–282.
Salvador, J. M., Mittelstadt, P. R., Guszczynski, T., Copeland, T. D., Yamaguchi, H., Appella, E., Fornace, A. J. & Ashwell, J. D. (2005). *Nature Immunol.* **6**, 390–395.
Shi, Y. & Gaestel, M. (2002). *Biol. Chem.* **383**, 1519–1536.
Stura, E. A., Chen, P., Wilmot, C. M., Arevalo, J. H. & Wilson, I. A. (1992). *Proteins*, **12**, 24–30.
Stura, E. A. & Wilson, I. A. (1990). *Methods*, **1**, 38–49.
Thaller, C., Weaver, L. H., Eichele, G., Wilson, E., Karlsson, R. & Jansonius, J. N. (1981). *J. Mol. Biol.* **147**, 465–469.
Tzarum, N., Diskin, R., Engelberg, D. & Livnah, O. (2011). *J. Mol. Biol.* **405**, 1154–1169.
Vagin, A. & Teplyakov, A. (2010). *Acta Cryst.* D**66**, 22–25.
Wang, Z., Harkins, P. C., Ulevitch, R. J., Han, J., Cobb, M. H. & Goldsmith, E. J. (1997). *Proc. Natl Acad. Sci. USA*, **94**, 2327–2332.
Widmann, C., Gibson, S., Jarpe, M. B. & Johnson, G. L. (1999). *Physiol. Rev.* **79**, 143–180.
Winn, M. D. *et al.* (2011). *Acta Cryst.* D**67**, 235–242.